Journal of Solar Energy Research (JSER)

Journal homepage: www.jser.ut.ac.ir

Two-Junction Silicon Vertical Solar Cells: A Comparison of Tunnel Junction and Metallic Contact Connections

Atabek Atamuratov[a], Bekhzod Jumaboev[a*], Ahmed Yusupov[b], Eldor Khaitboev[a], Makhkam Khalilloev[a], Jean Chamberlain Chedjou[c]

[a]*Physics department, Urgench State University, P.O. Box: 220100, Urgench, Uzbekistan*
[b]*Department of Electronics and Radiotechnics, Tashkent University of Information Technologies, P.O. Box: 200100, Tashkent, Uzbekistan*
[c]*Institute of Smart Systems Technologies, University of Klagenfurt, P.O. Box: 9020, Klagenfurt, Austria*

ARTICLE INFO

Article Type:

Research Article

Received:2026.02.13
Accepted in revised form:2026.06.03

Keywords:
Silicon Tunnel Junction; Two Junctions Solar Cell; Vertical Solar Cell; Efficiency of Solar Cell; Fill Factor

A B S T R A C T

In this work, the modelling of a two-junction vertical silicon solar cell is presented. The primary focus is on comparing the characteristics and performance parameters of the device when either a tunnel junction or a metallic layer is employed as the interconnect between the subcells. The advantages and limitations of fabrication technologies for vertical solar cells incorporating either a tunnel junction or a metallic interlayer as the inter-subcell contact are discussed. For the tunnel-junction-based structure, the simulation framework and set of parameters used in the modeling are described in detail. By fitting the simulated and experimental I-V characteristics of the tunnel junction, the following parameters were extracted: the effective masses at the band edges $m_c=0.212m_0$, $m_v=0.178m_0$, as well as the Huang–Rhys factor S=1.29. Comparative results for the dependence of conversion efficiency on solar concentration are also presented. It is shown that, for the considered geometrical dimensions, the efficiency differences between the analyzed device configurations are minimal. For both types of solar cells, the conversion efficiency increases approximately linearly with solar concentration up to approximately 200 suns, reaches a saturation region, and then begins to decrease at concentrations exceeding approximately 500 suns.

1. Introduction

One of the main trends in the development of electronics is designing electronic devices with low

*Corresponding Author Email: jumaboyevbexzod@urdu.uz

Cite this article: Atamuratov, A., Jumaboev, B., Yusupov, A., Khaitboev, E., Khalilloev, M. and Chedjou, J. C. (2026). Two-Junction Silicon Vertical Solar Cells: A Comparison of Tunnel Junction and Metallic Contact Connections. Journal of Solar Energy Research, 11(2), 3027-3040. doi: 10.22059/jser.2026.410974.1722

DOI: 10.22059/jser.2026.410974.1722

energy consumption and renewable energy sources, particularly solar cells. The development of low-energy electronic devices is mainly connected to miniaturization or scaling and to solving problems arising from this [1, 2]. A key goal in developing solar power devices is to enhance quality and efficiency while reducing or optimising costs. One approach to achieving this goal is to select suitable materials or develop innovative solar cell (SC) structures. Although many materials have been suggested for use in SC in recent years, silicon remains one of the most considered due to its extensive research, ongoing technological advancements, and decreasing cost. Designs aimed at enhancing SC efficiency include multijunction (MJ) SCs [3, 4] and concentrator systems that utilize specialized optical components to concentrate solar radiation [5, 6]. MJ SCs offer relatively high efficiency while reducing the need for costly semiconductor materials.

MJ SCs can have either horizontal or vertical architectures. Horizontal MJ SCs impose specific requirements on the optical properties of the constituent layers and on the ordering of the p–n junctions according to the band gaps of the semiconductor materials. Also, there are limitations to the contact area and series resistance. In vertical SCs, there are no such limitations, and one of the main advantages is a sufficiently low series resistance resulting from a large cross-section. Besides, vertical SCs have several substantial advantages over planar (horizontal) SCs [7]: (1) there are no controversial requirements for emitter resistance, spectral sensitivity or surface area contact; (2) they are transparent in long wavelengths because there are no metal layers on the front and back surfaces; (3) they can induce a high voltage (due to a connection in series of p-n junctions) and a low current at the same power. The latter advantage leads to an increase in solar cell (SC) efficiency, accompanied by a reduction in losses associated with the formation of high-current components.

In the manufacturing/fabrication of a monolithic multi-junction solar cell structure, metal layers (ML) [7, 8] and tunnel junctions (TJ) [9-11] can be used as contacts between the p-n junctions. Technologies of manufacturing SC using a metal layer and tunnel junction are considerably different and have their own advantages and challenges. The technology related to the use of a metal layer is relatively simple, but presents the following most critical challenges related to the mechanical stacking approach to integration [7, 12]:

- Post-growth bonding approaches are favorable; the bond interface would go through the high-temperature epitaxial growth process.
- The bonding temperature must be compatible with the metal and semiconductor material.
- In the case of horizontal MJ SC, the bonding layer should be thin and optically transparent.
- For the operation of a two-terminal solar cell under concentrated sunlight, it is crucial to realise electrically conductive connection/bond layers to avoid additional series resistance.
- The connection/bonding interfaces should have a low surface roughness and must be free from native oxides.
- When diffusion welding cells, sufficient pressure must be applied to produce the required plastic deformation of the metal layer without mechanically destroying the cells.

The use of tunnel junctions as an interconnect between subcells is more complex than mechanical stacking/bonding; however, it represents a more advanced approach that eliminates the limitations inherent to mechanical bonding methods. The use of tunnel junction technology can be divided into two approaches depending on the semiconductor materials used in MJ SCs.The first direction includes SC based on III-V semiconductors, and the second is based on Silicon. In MJ SCs based on III–V semiconductors, the use of tunnel junctions started relatively early, since tunnel diodes based on GaAs were first fabricated [13]. Therefore, the vast majority of works devoted to the use of a tunnel junction as a contact between p-n junctions in MJ SC refer to GaAs tunnel junctions.

Although the efficiency of Si-based SCs is lower than that of III–V semiconductor-based SCs, their significantly lower cost makes the development of Si-based MJ SCs highly important. The technology for fabricating Si tunnel diodes for c-Si-based tandem solar cells has been developed only relatively recently [14, 15], and consequently, the number of studies in this area remains limited. In [14, 15], it is suggested to use fast thermal diffusion with a low thermal budget for fabricating Si-based tunnel junctions.

To the best of our knowledge, although several experimental and theoretical (simulation) studies have investigated multijunction [16-18], particularly vertical multi-junction solar cells [7-10, 19, 20] using metal layers and tunnel junctions as intercell contacts, no research has yet compared the performance of these two types of solar cells. Moreover, there are very few studies on silicon-

based multi-junction vertical solar cells, although, in practice, most commercially deployed solar cells are still based on silicon.

This underscores the importance of this work, which seeks to advance the state of the art by thoroughly examining the performance of these two commonly used silicon-based solar cell types.

Experimental work on optimising the parameters of MJ SCs is costly and time-consuming. Therefore, developing simulation models that accurately describe the physical processes in SCs is crucial to accelerate the identification of optimal parameters for monolithic MJ SCs with silicon tunnel junctions. The simulation model should provide an effective and reliable method for studying multijunction SCs with tunnel junctions between solar cells as contacts. This work is devoted to the development of a simulation model of a silicon tunnel junction for application in vertical concentrator Si-based MJ SCs. The characteristics and parameters of a monolithic two-junction vertical SC with a tunnel junction will then be compared to those of a monolithic two-junction vertical SC with a metal layer as the contact between the p-n junctions.

"In our work, we focused mainly on comparing the characteristics of two transition vertical solar cells with a metal contact and a tunnel junction between the cells. In both cases, we chose the same constant temperature regime."

This paper is organised as follows: Section II presents the simulation model for the silicon tunnel junction, designed for application in two-junction vertical solar cells. Section III discusses the simulation results of monolithic vertical two-junction solar cells, utilizing tunnel junctions and metallic layers as contacts. Subsection III.A addresses the applied voltage distribution between cells in the vertical tunnel junction solar cell (VTJSC). Subsection III.B introduces the model and voltage distribution between cells in vertical metal layer solar cells (VMLSC). Subsection III.C compares the efficiencies of VTJSC and VMLSC under different solar concentrations. The last Section (Section IV) is devoted to concluding remarks.

2. Research Methodology

The research methodology consists of several consecutive stages. First, a structural model of a silicon tunnel junction was developed in the TCAD environment. Relevant physical models describing tunnelling processes in the junction were identified, and the simulation parameters necessary for accurate modeling of the tunnelling current were determined. The validity of the model was verified by comparing the simulated current–voltage characteristics with the corresponding experimental data.

In the next stage, a structural model of a two-junction silicon solar cell was developed. Two types of vertical two-junction solar cell structures were then simulated: one employing a metallic layer as an interconnection contact between the subcells (VMLSC), and another using a tunnel junction as an interconnection contact (VTJSC).

Further simulations were performed to analyse the voltage distribution between the subcells and the interconnection layer in both structures. In the case of VTJSC, the voltage distribution across the subcells and tunnel junction was investigated, and the dependence of cell efficiency on solar concentration was evaluated. For the VMLSC structure, the voltage distribution between the subcells and the metallic interconnection layer was analysed, and simulation parameters were determined to ensure accurate modelling of its current–voltage characteristics. The simulated I–V characteristics were then compared with the available experimental data.

Finally, the efficiency dependence on solar concentration was calculated for both structures, and a comparative analysis of the VTJSC and VMLSC performance was carried out. A flowchart to show the methodology procedure is shown in Figure 1.

3. Simulation model for silicon tunnel junction

To simulate the I-V characteristics of a two-junction solar cell with a tunnel junction as the contact, we first define the simulation model for the tunnel junction (TJ). The model was developed in the TCAD Sentaurus Synopsys environment and calibrated by comparing it with experimental results presented in [21]. The experimental tunnel junction was made based on the rapid thermal diffusion from the spin-on diffusants technology. The tunnel junction was formed on a Si(100) substrate with a resistivity of 1-5 kΩ, and the doping level of the n- and p-regions was 10^{20} cm^{-3}.

The structure of the simulated tunnel junction is shown in Figure 2, with the parameters and geometric dimensions matching those of the experimental setup [21], as listed in Table 1. The only exception is the junction height: in the experimental setup, the height, H, and thickness, T, of the junction are 16 μm and 4 μm, respectively. As we consider a 2D simulation, the thickness of structures by default is selected equal to 1 μm. To ensure that the areas are equivalent, the height of the simulated junction is chosen to be 64 μm.

According to [22], the nonlocal tunnelling model provides the most accurate description of carrier tunnelling through tunnel junctions. In this work, the tunnelling process was described using the nonlocal Band-to-Band tunnelling model implemented in TCAD Sentaurus.

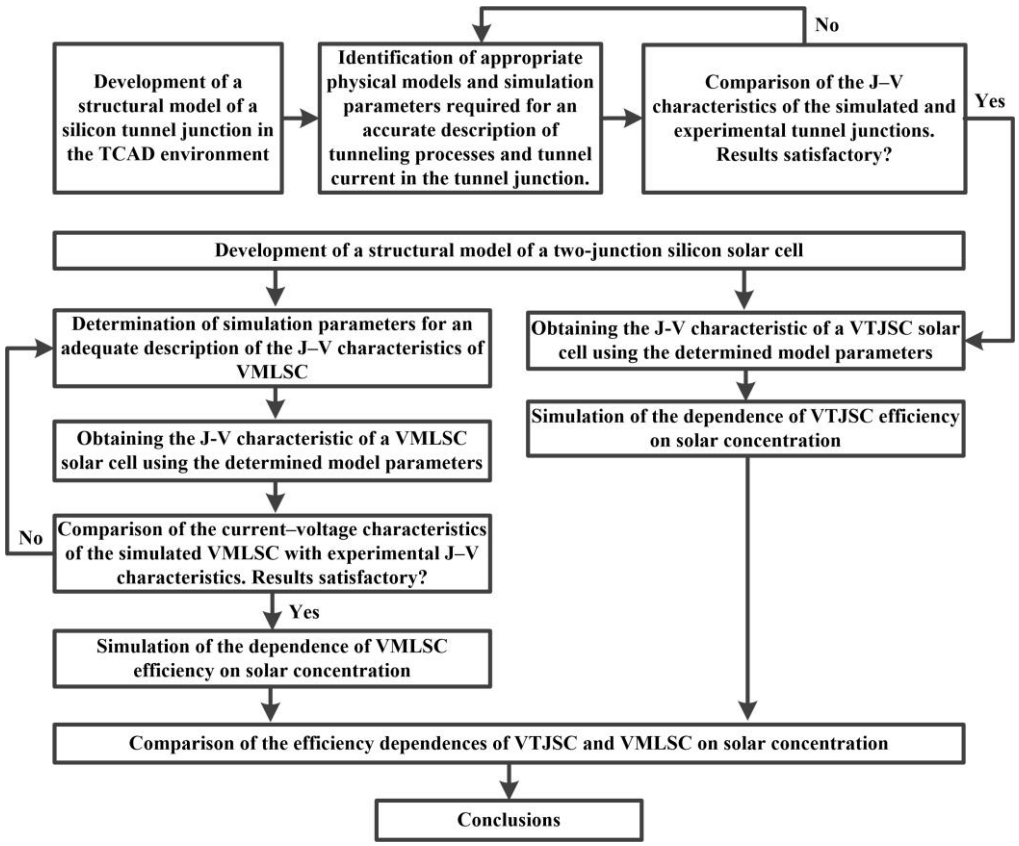

Figure 1. A flowchart of the methodology procedure

The diffusion component of the current is described by the drift-diffusion transport model, which is defined by the Poisson Equation and the Continuity Equation, where current densities for electrons and holes are given by known formulas 1 and 2 taken from [23]:

$$\vec{J}_n = -nq\mu_n \nabla\Phi_n - q\mu_n kT\nabla n \quad (1)$$

$$\vec{J}_p = -pq\mu_p \nabla\Phi_p + q\mu_p kT\nabla p \quad (2)$$

where n and p are electron and hole concentrations, μ_n and μ_p are the electron and hole mobilities, Φ_p and Φ_n are the electron and hole quasi-Fermi potentials, respectively, q is the elementary charge, k is the Boltzmann constant, and T is the absolute temperature. In this model, the Schokly-Read-Hall (SRH) recombination mechanism and mobility dependence on the doping level are accounted for.

The quantities indicated in Table 1 are shown in Figure 2, where H is the height of the tunnel junction; W_{p+}, W_{p++}, and W_{n++} are the widths of p^+, p^{++}, and n^{++} layers, respectively; p^+, p^{++}, and n^{++} are the doping levels in the appropriate layers.

In accordance with the Band-to-Band tunnelling model and based on the findings from [24], the tunnelling probability depends on the masses of the zone edges, m_c and m_v. To calibrate the model, the J-V curve of the tunnel junction was simulated for various values of m_c and m_v, and compared with the experimental data. The masses m_c and m_v primarily affect the amplitude of the tunnel current. The amplitudes of the tunnel currents, specifically, the portions of the J-V curve from zero voltage up to the first maximum, were found to match between the simulated and experimental tunnel junctions when $m_c=0.212m_0$ and $m_v=0.178m_0$. A change in these masses changes the amplitude of the tunnel current, but it does not change the voltage drop across the tunnel junction [22]. Therefore, a change in the tunnelling masses does not change the voltage distribution between the subcells and the tunnel

junction, and therefore does not change the current density-voltage characteristic and parameters of the two-junction solar cell.

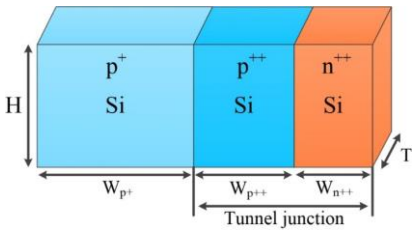

Figure 2. The structure of the simulated silicon tunnel junction (TJ)

Table 1. Parameters and geometrical sizes of the simulated tunnel junction (TJ)

Structure parameters	Value
H (μm)	64
W_{p+} (μm)	0.05
W_{p++} (μm)	0.02
W_{n++} (μm)	0.014
p^+ (cm^{-3})	1e18
p^{++} (cm^{-3})	2e20
n^{++} (cm^{-3})	1.1e20

The tunnelling effective mass plays a significant role only at low doping levels in the tunnel junction, where the junction resistance becomes comparable to that of the subcells. At sufficiently high doping levels, the tunnel junction resistance becomes very small, the voltage drop across it is negligible, and the junction behaves similarly to an ohmic contact.

The pre-factors for the Richardson constants are g_c=2.1 and g_v=0.66, as derived from [25].

The slopes of the J–V curves are determined by the series resistance RSR_SRS, which arises from the bulk resistance of the base region and the contact resistance [22, 25]. At R_S=275 Ω, the slopes of the simulated and experimental J-V are in good agreement. According to [22, 25], to match the diffusion component of the simulated tunnel junctions' J-V characteristics with the experimental data, it is necessary to include trap-assisted tunnelling in addition to direct band-to-band tunnelling. Trap-assisted tunnelling describes the dependence of lifetimes t_n and t_p on the field by the factor [26]:

$$\tau_c = \tau_{dop} \frac{f(T)}{1+g_c(F)} \tag{3}$$

where c=n or c=p, in Shokley-Read-Hall recombination [26, 27]:

$$R_{net}^{SRH} = \frac{np - n_{i,eff}^2}{\tau_p(n+n_1)+\tau_n(p+p_1)} \tag{4}$$

with

$$n_1 = n_{i,eff} \exp\left(\frac{E_{trap}}{kT}\right) \tag{5}$$

$$p_1 = n_{i,eff} \exp\left(\frac{-E_{trap}}{kT}\right) \tag{6}$$

where E_{trap} is the difference between the defect level and intrinsic level, n and p are electron and hole concentrations, respectively, $n_{i,eff}$ is the effective intrinsic concentration, k is the Boltzmann constant, and T is an absolute temperature; the field dependence of the recombination rate is taken into account by the following field enhancement factor [26]:

$$\left[1+g\left(F\right)\right]^{-1} \tag{7}$$

of the SRH lifetimes in (3) [28]. In the Schenk Trap-Assisted Tunnelling field enhancement model, which we used in simulation, factor g(F) depends on the lattice relaxation energy $\varepsilon_R = S\hbar\omega_0$, where S is the Huang–Rhys factor, $\hbar\omega_0$ is the effective phonon energy [28]. The simulation model was calibrated by comparing the dependencies of lifetimes on the field carried out from our simulation and the theoretical Schenk model [28] for different relaxation energies and different phonon energies (Figure 3). The good agreement between simulation and theoretical results is seen in the figures.

To reach a good agreement in the diffusion component in the J-V curve of TJ, we implemented the Huang–Rhys factor S as well as in [24, 29]. A good agreement between the diffusion components of the experimental and simulated tunnel junctions is achieved for S = 1.29. The Huang–Rhys factor S, as well as the tunnelling effective masses, plays a significant role only at low doping levels of the tunnel junction, where the junction resistance becomes comparable to the resistance of the subcells. The Huang–Rhys factor S affects the diffusion current of the tunnel junction. This current appears at high voltages (in our case, greater than 0.4 V) applied to the tunnel junction. However, since the resistance of the tunnel junction in the tunnel current mode is much lower than the resistance of the p-n junctions, a small voltage (in our case, less than 0.2 V) is applied to the tunnel junction, which is

insufficient to induce a diffusion current. Therefore, the S factor has a minimal impact on the performance of a two-junction solar cell.

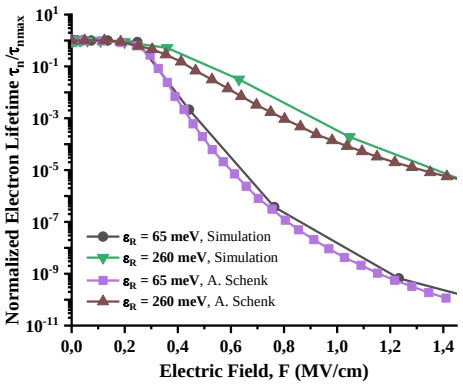

(a)

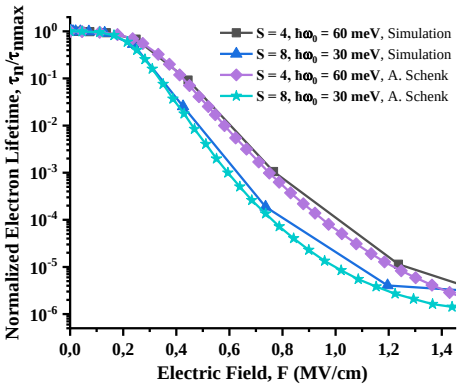

(b)

Figure 3. Normalised lifetimes dependence on the field for different relaxation energy ε_R (a) and for different phonon energy $\hbar\omega_0$ (b)

Table 2 summarizes the parameters used in the simulations and the corresponding references validating the selected parameter values. The significant difference in the S parameter is likely due to the inclusion of trap levels in the trap-assisted tunnelling model; it only affects the diffusion part of the tunnel junction current, which is not active during the solar cell's operation. The resulting J-V characteristics of the simulated tunnel junction, using the aforementioned parameter values, are shown in Figure 4 and compared with the experimental J-V curve presented in [19]. For comparison, the current in the experimental results has been recalculated (say converted) to current density.

The discrepancy between the currents observed in the voltage range from 0.2 to 0.5 V arises from the fact that the current model does not account for trap-assisted tunnelling through defect states located at different energy levels within the band gap [22, 25]. However, as will be shown later, in section III A, the voltage dropped on the tunnel junction in the solar cell is very low (near zero). Therefore, the portion of the J–V curve corresponding to voltages above 0.2 V does not significantly affect the characteristics and performance parameters of the solar cell.

In summary, this section has defined the key tunnel junction simulation parameters, which will be used in the subsequent simulation of vertical two-junction monolithic solar cells with a tunnel junction in Section 4 A.

Table 2. Parameters used in the simulation of the considered TJ

Parameters	Values of parameters used in this work	Values of parameters used in reference works	Ref.
m_C/m_V (m_0)	0.212/0.178	0.2/0.2	[21]
g_C/g_V (-)	2.1/0.66	2.1/0.66	[21]
S (-)	1.29	0.3	[30]
R_S (mΩ·cm^2)	0.9	2	[21]

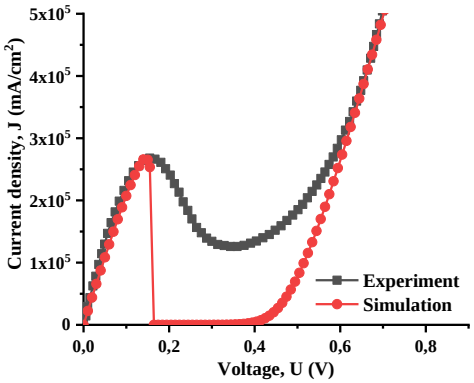

Figure 4. J-V characteristics of the simulated and experimental silicon tunnel junctions

4. Simulation of monolithic vertical two-junction solar cells with tunnel junction and metallic layer as contacts

In this section, the tunnel junction simulation model developed in Section 3 is used to simulate a monolithic two-junction concentrator vertical solar cell with a tunnel junction as the contact between the subcells (VTJSC) at various solar concentrations. The results are then compared with the efficiency dependence on solar concentration for a monolithic

two-junction concentrator vertical solar cell with a metal layer as the contact (VMLSC).

A. Applied voltage distribution between cells in VTJSC

The key requirement for the contact between individual solar cells (p-n junctions) in a monolithic multi-junction solar cell is that the differential resistance must be small compared to the resistance of the individual solar cells connected in series. This ensures that the voltage applied to the monolithic solar cell is mainly dropped across the p-n junctions. Additionally, the contact resistance should not distort the J-V curve of the single p-n junctions. Therefore, the contact must be Ohmic (linear) within the active voltage range of the multi-junction solar cell. This condition is crucial for achieving a high fill factor (FF) and, consequently, high efficiency of the solar cell. In this work, the characteristics and parameters of the monolithic two-junction VTJSC and VMLSC are compared. The structure of the two-junction solar cell with the tunnel junction is shown in Figure 5, and the parameters are presented in Table 3. The height (H) of the solar cell has been chosen according to the value given to the size of the tunnel junction described earlier (see section 3).

Table 3. Parameters of the two-junction solar cell (SC) with tunnel junction (TJ)

Structure parameters	Value
H (μm)	64
W_{n+} (μm)	5
W_n (μm)	185
W_{p+} (μm)	5
W_{p++} (μm)	0.02
W_{n++} (μm)	0.014
n^+ (cm^{-3})	1e19
n (cm^{-3})	1e14
p^+ (cm^{-3})	1e18
p^{++} (cm^{-3})	2e20
n^{++} (cm^{-3})	1.1e20

In the active mode of a multi-junction solar cell, the distribution of the applied voltage between the p-n junctions and the contact layer between the cells plays a crucial role. This distribution affects the fill factor of the solar cell characteristics, which in turn impacts its efficiency. To determine the voltage distribution between the cells and the tunnel junction, the differential resistances of the solar cells (p-n junctions) and the tunnel junction must be calculated at different voltages.

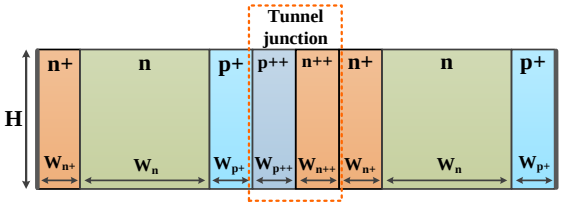

Figure 5. Structure of the two-junction solar cell, with the tunnel junction (TJ) acting as the contact between the single elements. H = 64 μm

These differential resistances are calculated from the J-V curves of the solar cell components/elements (p-n junctions) and the tunnel junction. The dependence of the differential resistances of the tunnel junction and the single p-n junction (SC element) on the applied voltage, as calculated from the simulated I-V curves, is shown in Figure 6.

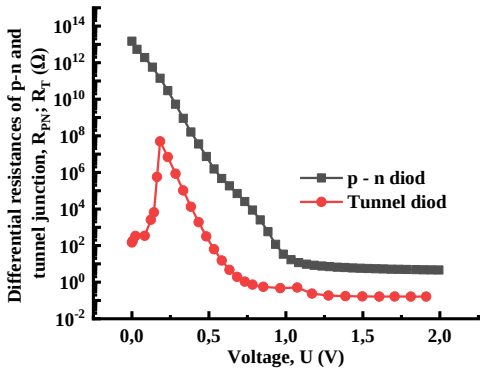

Figure 6. Dependences of differential resistances of p-n-junction and tunnel junction (TJ) on the applied voltage

Based on the dependencies shown in Figure 5, the voltage distribution between the elements and the tunnel junction in the two-junction solar cell was calculated. The calculation was performed using the equivalent circuit of SC shown in Figure 7. The resulting voltage distribution is shown in Figure 8. The figure demonstrates that, for values up to 1.5 V, nearly the entire applied voltage is dropped across the solar subcells.

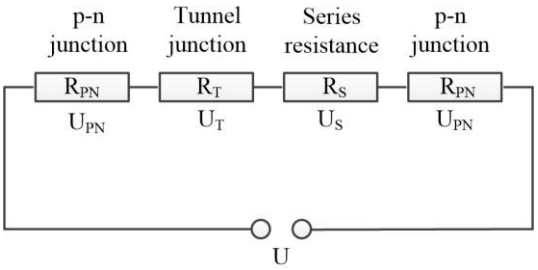

Figure 7. Equivalent circuit of a two-junction solar cell with a tunnel junction as the contact and with series resistance. R_{pn}, R_T, R_S, and U_{pn}, U_T, U_S represent the resistances and the voltages dropped across the p-n-junction, tunnel junction, and series resistances, respectively.

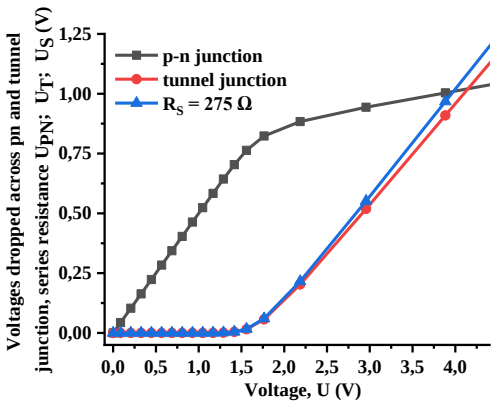

Figure 8. Dependence of the voltages U_{pn}, U_{TJ} и U_S, dropped across each p-n-junction, TJ tunnel junction, and series resistance (R_S), respectively, on the applied voltage U in a two-junction solar cell. R_S (VMJSC) = 1093.75 Ω; R_S (VTJSC) = 275 Ω

B. Simulation model and voltage distribution between cells in VMLSC

For comparison, a two-junction solar cell with a metal layer as the contact between subcells was considered. The parameters of this solar cell were chosen to match those of the SC with a tunnel junction. The simulations were performed using a drift–diffusion transport model incorporating SRH, Auger, radiative, and surface SRH recombination mechanisms, together with a mobility model accounting for doping-dependent carrier mobility. The model used for simulation was calibrated by comparing the J-V curves obtained from the simulation with experimental data presented in [8] (Figure 9). The series resistance for the SC parameters used, which has led to a good agreement between the J-V curves of the VMLSC and the experimental one, was R_S = 140 Ω. In this case, the height of the experimental structure, as well as that of the simulated structure, was equal to 500 μm. However, when comparing the characteristics of VMLSC and VTJSC, the height of the VMLSC structure was chosen to match that of the VTJSC, with a height of H=64 μm. As a result of this size change, the series resistance of VMLSC was also adjusted to the value R_S = 1093 Ω.

When using a metal layer as the contact between the cells, it must be taken into account (or considered) that its resistance, unlike the dynamic resistance of a tunnel junction, depends solely on the geometric dimensions and the material, and does not depend on the applied voltage. In the simulation of the two-junction VMLSC, the thickness of the metal layer was set equal to W_{met} = 55 μm, consistent with the experimental solar cell reported in [8].

The distribution of the applied voltage between the solar cells (SCs), the metal layer, and the series resistance was determined using the same electrical circuit shown in Figure 7. However, instead of the tunnel junction resistance, the resistance of the metal layer was included in the circuit. The results of the voltage distribution estimation in the mentioned electrical circuit are shown in Figure 10. The figure shows that, in the case of VMJSC, as well as in the case of VTJSC, the applied voltage predominantly drops across the solar cells (p-n junctions) up to a value of approximately 1.5 V.

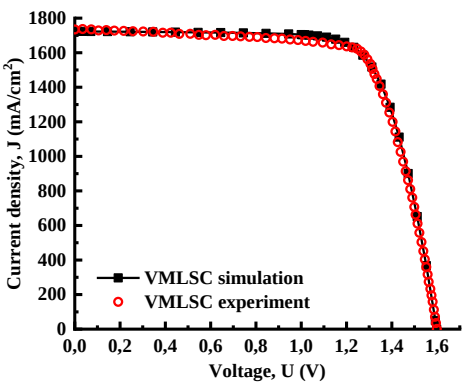

Figure 9. Comparison of the I-V curves for the simulated and experimental solar cells [8] with a metal layer as the contact between cells. H = 500 μm, R_S = 230 Ω, and a solar concentration of 2108 Suns

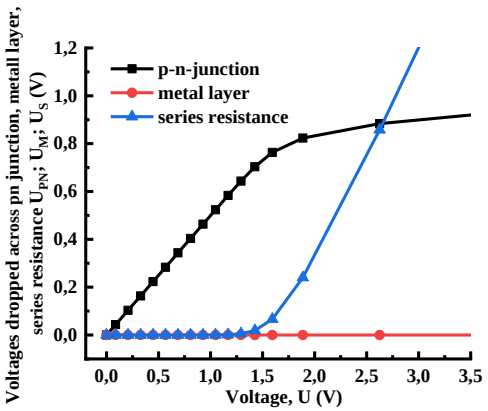

Figure 10. Dependence of the voltages dropped across the cell (p-n-junction), metal layer, and series resistance on the applied voltage, with H = 64 μm and R_S = 1093.75 Ω

C. Comparison of VTJSC and VMLSC efficiencies at different solar concentrations

To assess the advantages and disadvantages of VTJSC, the efficiencies of both VTJSC and VMLSC were compared as a function of solar concentration. The simulation results show that, for both types of solar cells, the efficiency increases nearly linearly with solar concentration up to 200 Suns, reaching approximately 20.4%. Beyond this point, the efficiency levels off, i.e., reaches saturation (Figure 11). For both solar cells, the efficiency begins to decrease at a concentration of 500 Suns.

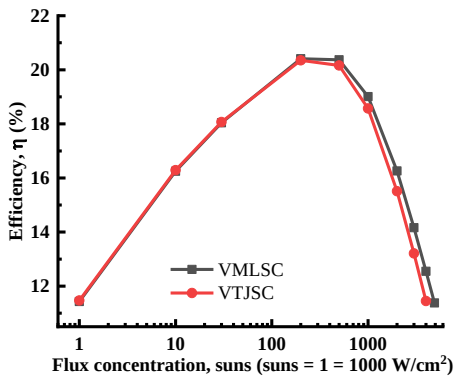

Figure 11. Dependence of the efficiencies of VTJSC and VMLSC on solar concentration, with H = 64 μm, R_S (VMLSC) = 1093.75 Ω, and R_S (VTJSC) = 1368.75 Ω

The increase in efficiency with solar concentration up to 200 Suns for both types of solar cells is attributed to a linear rise in the short-circuit current and a gradual (or monotonous) increase in the open-circuit voltage, followed by saturation (Figure 12). The observed efficiency decline is due to a reduction in the fill factor at solar concentrations above 200 Suns (Figure 13). This is because, at solar concentrations above 200 Suns, the distribution of the applied voltage changes: a larger portion is dropped across the series resistance, reducing the voltage drop across the solar cell, which in turn leads to a reduction in the fill factor (FF). Since the series resistance in VTJSC is higher than in VMLSC, this leads to a comparatively larger reduction in the fill factor and, consequently, a more significant drop in efficiency.

Although the efficiency behaviour of both types of solar cells is similar, the efficiency difference between VTJSC and VMLSC increases linearly as the solar concentration exceeds 200 Suns.

VTJSC efficiency decreases faster than that of VMLSC, so with a solar concentration of 500 Suns,

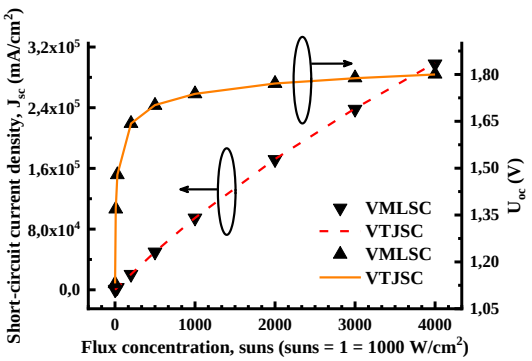

Figure 12. Dependencies of the short-circuit current density and open-circuit voltage on solar concentration for VTJSC and VMLSC, with H = 64 μm, R_S (VMLSC) = 1093.75 Ω, and R_S (VTJSC) = 1368.75 Ω

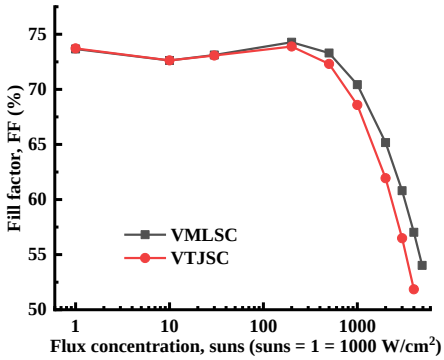

Figure 13. Dependence of the fill factor (FF) on solar concentration for VTJSC and VMLSC, with H = 64 μm, R_S (VMLSC) = 1093.75 Ω, and R_S (VTJSC) = 1368.75 Ω

the efficiency difference is 0.21% and with a concentration of 4000 Suns, 1.1%. Table 4 shows the difference in the efficiencies of VTJSC and VMLSC at different solar concentrations.

Table 4. Difference of efficiencies for VMLSC and VTJSC versus Solar concentration

Solar concentration, Suns	200	500	1000	2000	3000	4000
Difference of efficiencies for VMLSC and VTJSC, %	0.06	0.21	0.44	0.75	0.95	1.10

5. Validation of the results

To validate the obtained results, we compared the current–voltage characteristics and efficiencies of the simulated VTJSC and VMLSC with selected published data for silicon-based multi-junction vertical solar cells.

For comparison, two experimental vertical multi-junction silicon solar cells with metallic interconnects between subcells are reported in Refs. [7, 8], were considered. The number of junctions (subcells) in these studies differs from that in the device modelled in this work: Ref. [8] employs 40 subcells, whereas Ref. [7] uses 4. The geometrical dimensions of the subcells in our simulated structure were chosen to match those of the experimental device reported in Ref. [8], while the dimensions of the device in Ref. [7] differ. In addition, the reported experimental current density–voltage characteristics were obtained under different levels of solar concentration. To enable a consistent comparison, the experimental data were normalised with respect to solar concentration (2108 Suns), the number of subcells (two junctions), and the geometrical dimensions.

Figure 14 presents the J–V characteristics of the simulated VTJSC and VMLSC alongside the normalised J–V curves of the two experimental samples. As can be seen, the photo-generated current densities are of the same order of magnitude.

The observed discrepancies between the simulated J–V characteristics and those reported in Ref. [7] are most likely attributable to differences in the doping levels within the subcells and in the series resistance.

Table 5 compares the short-circuit current density, open-circuit voltage, fill factor, and efficiency of the simulated and experimental solar cells extracted from J-V curves shown in Figure 14. As can be seen, there is good agreement between the simulation results and the experimental data, indicating the adequacy and reliability of the model employed in this work.

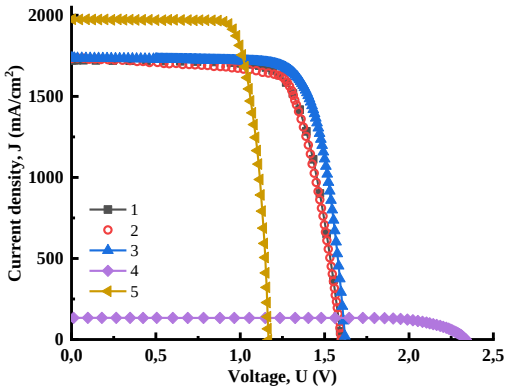

Figure 14. J-V curves of vertical multi-junction Si solar cells, carried out from experimental and simulation works: 1–simulated VMLSC (this work); 2 – experimental VMLSC, normalised to 2108 Suns and on two junctions [8]; 3–simulated VTJSC (this work); 4–experimental, not normalised VMLSC [7]; 5–J-V curve for VMLSC carried out from experimental work [7] by normalisation to 2108 Suns and on two junctions

Table 5. Comparative analysis of parameters of vertical multi-junction Si solar cells, including different experimental and simulation studies

Structure	J_{SC} [mA/cm^2]	U_{OC} [V]	FF [%]	η [%]	Ref.
VMLSC	1734	1.59	73.38	19.19	[8]
VMLSC	1975	1.16	79.67	17.39	[7]
VMLSC	1723	1.59	73.25	19.14	This work
VTJSC	1737	1.62	76.93	20.56	This work

6. Conclusions

In this work, the simulation parameters and models for silicon tunnel junctions (TJs) used in vertical two-junction solar cells were established. Specifically, the masses of zone edges m_c and m_v, along with the Huang-Rhys coefficient S, were defined to accurately characterise the amplitude and diffusion components of the tunnel current in a silicon tunnel junction.

The simulation results show that the efficiency dependence on solar concentration for VTJSC and

VMJSC is nearly identical. In both cases, efficiency increases linearly with solar concentration up to 200 Suns, reaches a saturation point, and then begins to decline at concentrations above 500 Suns. Since the efficiencies of VTJSC and VMJSC are practically the same, the choice between using a tunnel junction or a metal layer as the contact between solar cells in the development of monolithic silicon vertical multi-junction solar cells should be based on an assessment of the complexity and cost of the production technology. It is also crucial to ensure that the chosen technology maintains a low series resistance.

Although the use of a tunnel junction or a metal layer between the cells of a multi-junction solar cell has advantages and disadvantages, it is also necessary to take into account the technological tolerances in the fabrication of these solar cells. Indeed, when manufacturing multi-junction solar cells with a tunnel junction between subcells, it is necessary to control some parameters and conditions for obtaining a tunnel junction, which may affect the characteristics of the solar cell. In particular, a decrease in the level of doping of tunnel junctions can lead to an increase in the width of the junction and, accordingly, to a decrease in tunnel current, which is equivalent to an increase in the contact resistance between the subcells of the solar cell. This, in turn, can lead to a deterioration in the performance of the solar cell. In addition, the doping profiles of the n^{++}/p^{++} layers must be properly designed to allow efficient charge transport in a monolithic tandem solar cell. A higher and more abrupt doping of the n^{+} layer increases the B2B tunnelling current [25]. The substrate on which the tunnel junction is made also matters. A junction made on an n^{+} substrate shows a lower amplitude of the tunnelling current density compared to a junction made on a p^{+} substrate [14].

When fabricating multi-junction solar cells with a metal interlayer between the subcells, several factors must be taken into consideration. One of these is the establishment of a Schottky barrier between the metal and the semiconductor, which can significantly affect the characteristics and performance of the solar cell. To avoid this, it is necessary to provide appropriate additional doping of the semiconductor layer that is in contact with the metal. Additionally, it is important to select a metal material that remains stable during subsequent thermal processing and under extreme operating temperature conditions. For example, a large mismatch in thermal expansion coefficients can lead to mechanical stress and dislocation formation, thereby affecting the current–voltage characteristics of the solar cell. It is also important to consider the compatibility of the metal layer with the solar cell manufacturing technology. If the solar cell manufacturing technology involves annealing and passivation at temperatures above 300-500 C, it may result in the diffusion of metal atoms into the semiconductor layer, leading to the formation of defects.

One of the primary objectives of this work was to develop a simulation model for the tunnel junction used as an interconnect between the subcells of a solar cell. The proposed model accurately captures the rising (left) branch of the tunnelling current as well as the diffusion current of the tunnel junction; however, it does not reproduce the decreasing (right) branch of the tunnel current in the I–V characteristic (Figure 4).

Nevertheless, the voltage drop across the tunnel junction in a two-junction solar cell lies within the rising region (i.e., the left branch) of the tunnelling current. Therefore, the proposed model can adequately describe the current density–voltage characteristics of a two-junction solar cell incorporating a tunnel junction. In addition, the analysis of the tunnelling current models performed in this work may be useful for selecting appropriate models for the simulation of various tunnelling-current-based devices [31, 32]. Despite this, future work will focus on developing a comprehensive model capable of accurately describing the J–V characteristics of the tunnel junction for applications in multi-junction solar cells as well as in other nanoscale semiconductor devices.

Acknowledgments

The authors thank the research department of Urgench State University for their support in conducting this research.

Nomenclature

2D	Two Dimensional
c	Carrier type index (n or p) (-)
E_{trap}	Trap energy level (eV)
F	Electric field (V/cm)
FF	Fill factor (%)
f(T)	Temperature dependent factor (-)
g(F)	electric-field enhancement factor (-)

g_C/g_V	Prefactors (-)
H	Height of tunnel junction (μm)
J_n/J_p	Current densities for electrons and holes (mA/cm^2)
J_{sc}	Short-circuit current density (mA/cm^2)
k	Boltzmann constant (J/K)
m_c	conduction-band tunnelling mass (-)
m_v	valence-band tunnelling mass (-)
MJ	Multijunction
ML	Metal layer
n/p	Electron and hole concentrations (cm^{-3})
n_1	Electron trap density parameter (cm^{-3})
$n_{i,eff}$	Effective intrinsic carrier concentration (cm^{-3})
n^{++}	Doping concentration in n^{++} layer (cm^{-3})
p^+	Doping concentration in p$^+$ layer (cm^{-3})
p^{++}	Doping concentration in p^{++} layer (cm^{-3})
p_1	Hole trap density parameter (cm^{-3})
q	Elementary charge (C)
Rs	series resistances (Ω)
R_{SRH}	Shockley–Read–Hall recombination rate (cm^{-3}·s)
SC	Solar cell
S	Huang–Rhys factor (-)
SRH	Schokly – Read - Holl
$suns$	Concentration of incident light (W/cm^2)
$TCAD$	Technology Computer – Aided Design
TJ	tunnel junction
T	Absolute temperature (K)
U_S	Voltage dropped across the series resistance (V)
U_T	Voltage dropped across the tunnel junction (V)
U_{pn}	Voltage dropped across the p-n-junction (V)
$VMLSC$	Vertical metal-layer solar cells
$VTJSC$	Vertical tunnel junction solar cell
V_{oc}	Open-circuit voltage (V)
W_{p+}	Width of p$^+$ layer (μm)
W_{p++}	Width of p^{++} layer (μm)
W_{n++}	Width of n^{++} layer (μm)
μ_n/μ_p	Electron and hole mobilities (cm^2/(V·s))
∇	Gradient operator (cm^{-1})
∇_n	Gradient of electron concentration (cm^{-4})
∇_p	Gradient of hole concentration (cm^{-4})
Φ_n/Φ_p	Electron and hole quasi-Fermi potentials (V)
η	Efficiency (%)
τ	Lifetime (s)
τ_c	Carrier lifetime (electron or hole lifetime) (s)
τ_{dop}	Doping-dependent lifetime (s)
τ_n	Electron lifetime (s)
τ_p	Hole lifetime (s)
ε_R	Relaxation energy (J)

References

[1] Atamuratov, A. E., Jabbarova, B. O., Khalilloev, M. M., Rajapov, D. R., Yusupov, A., Chedjou, J. C., Blugan, G., & Saidov, K. (2025). Impact of source (drain) doping profiles and channel doping level on self-heating effect in FinFET. *Micro and Nanostructures*, *197*, 208015. https://doi.org/10.1016/j.micrna.2024.208015

[2] Atamuratov, A. E., Yusupov, A., Atamuratova, Z. A., Chedjou, J. C., & Kyamakya, K. (2020). Lateral Capacitance–Voltage Method of NanoMOSFET for Detecting the Hot Carrier Injection. *Applied Sciences*, *10*(21), 7935. https://doi.org/10.3390/app10217935

[3] Atamuratov, A., Jumaboyev, B., Yusupov, A., Abdikarimov, A., & Loureiro, A. (2022). The effect of geometrical sizes on efficiency of vertical silicon tunnel junction solar cell for high solar concentration. 2022 International Conference on Information Science and Communications Technologies (ICISCT), https://doi.org/10.1109/ICISCT55600.2022.10146907

[4] Atamuratov, A., Jumaboyev, B., Abdikarimov, A., Yusupov, A., & Loureiro, A. (2023). The Effect of Height on the Efficiency of Vertical Silicon Tunnel Junction Solar Cell for High Solar Concentration. 2023 14th Spanish Conference on Electron Devices (CDE), https://doi.org/10.1109/CDE58627.2023.10339414

[5] Ferrer-Rodríguez, J. P., Fernández, E. F., Almonacid, F., & Pérez-Higueras, P. (2016). Optical design of a 4-off-axis-unit Cassegrain ultra-high concentrator photovoltaics module with a central receiver. *Optics Letters*, *41*(9), 1985–1988. https://doi.org/10.1364/OL.41.001985

[6] Shanks, K., Ferrer-Rodriguez, J. P., Fernández, E. F., Almonacid, F., Pérez-Higueras, P., Senthilarasu, S., & Mallick, T. (2018). A> 3000 suns high concentrator photovoltaic design based on multiple Fresnel lens primaries focusing to one

central solar cell. *Solar Energy*, *169*, 457–467. https://doi.org/10.1016/j.solener.2018.05.016

[7] Guk, E., Nalet, T., Shvarts, M., & Shuman, V. (1997). Characteristic features of silicon multijunction solar cells with vertical pn junctions. *Semiconductors*, *31*(7), 726–727. https://doi.org/10.1134/1.1187077

[8] Sater, B. L., & Sater, N. D. (2002). High voltage silicon VMJ solar cells for up to 1000 suns intensities. Conference Record of the Twenty-Ninth IEEE Photovoltaic Specialists Conference, 2002., https://doi.org/10.1109/PVSC.2002.1190778

[9] Geisz, J., Olson, J., Friedman, D., Jones, K., Reedy, R., & Romero, M. (2005). Lattice-matched GaNPAs-on-silicon tandem solar cells. Conference Record of the Thirty-first IEEE Photovoltaic Specialists Conference, 2005., https://doi.org/10.1109/PVSC.2005.1488226

[10] Derendorf, K., Essig, S., Oliva, E., Klinger, V., Roesener, T., Philipps, S. P., Benick, J., Hermle, M., Schachtner, M., & Siefer, G. (2013). Fabrication of GaInP/GaAs//Si solar cells by surface activated direct wafer bonding. *IEEE Journal of Photovoltaics*, *3*(4), 1423–1428. https://doi.org/10.1109/JPHOTOV.2013.2273097

[11] Mailoa, J. P., Bailie, C. D., Johlin, E. C., Hoke, E. T., Akey, A. J., Nguyen, W. H., McGehee, M. D., & Buonassisi, T. (2015). A 2-terminal perovskite/silicon multijunction solar cell enabled by a silicon tunnel junction. *Applied Physics Letters*, *106*(12). https://doi.org/10.1063/1.4914179

[12] Jain, N., & Hudait, M. K. (2014). III–V multijunction solar cell integration with silicon: Present status, challenges and future outlook. *Energy Harvesting and Systems*, *1*(3-4), 121–145. https://doi.org/10.1515/ehs-2014-0012

[13] Esaki, L. (1958). New phenomenon in narrow germanium p− n junctions. *Physical review*, *109*(2), 603. https://doi.org/10.1103/PhysRev.109.603

[14] Fave, A., Lelièvre, J.-F., Gallet, T., Su, Q., & Lemiti, M. (2017). Fabrication of Si tunnel diodes for c-Si based tandem solar cells using proximity rapid thermal diffusion. *Energy Procedia*, *124*, 577–583. https://doi.org/10.1016/j.egypro.2017.09.281

[15] Wang, J., Wheeler, D., Yan, Y., Zhao, J., Howard, S., & Seabaugh, A. (2002). Silicon tunnel diodes formed by proximity rapid thermal diffusion. Proceedings. IEEE Lester Eastman Conference on High Performance Devices, https://doi.org/10.1109/LED.2002.807706

[16] Bae, J., Yousuf, H., Khokhar, M. Q., Madara, P. C., Jang, S., Chu, M., Aida, M. N., Jony, J. A., Kim, E., & Park, S. (2025). High-efficiency mechanically stacked bifacial III-V/HJT multijunction solar cell enabled by spectral albedo. *Sustainable Energy Technologies and Assessments*, *83*, 104616. https://doi.org/10.1016/j.seta.2025.104616

[17] Zhang, J., Wang, R., Zhao, W., Zhang, H., Xu, Y., Wang, J., Zhong, X., Shen, F., Yao, L., & Ren, H. (2025). Guided growth of vertically aligned 2D perovskites improves the performance of monolithic perovskite/organic tandem solar cells. *Chemical Engineering Journal*, 170523. https://doi.org/10.1016/j.cej.2025.170523

[18] Im Noh, Y., Kim, C. U., & Choi, K. J. (2025). Perovskite/Homojunction-silicon tandem solar cells with optimized silicon nitride passivation and advanced double-sided ohmic contacts. *Materials Today Energy*, *52*, 101917. https://doi.org/10.1016/j.mtener.2025.101917

[19] Pozner, R., Segev, G., Sarfaty, R., Kribus, A., & Rosenwaks, Y. (2012). Vertical junction Si cells for concentrating photovoltaics. *Progress in Photovoltaics: Research and applications*, *20*(2), 197–208. https://doi.org/10.1002/pip.1118

[20] Xing, Y., Han, P., Wang, S., Fan, Y., Liang, P., Ye, Z., Li, X., Hu, S., Lou, S., & Zhao, C. (2013). Performance analysis of vertical multi-junction solar cell with front surface diffusion for high concentration. *Solar Energy*, *94*, 8–18. https://doi.org/10.1016/j.solener.2013.04.030

[21] Yan, Y. (2008). *Silicon-based tunnel diode technology*. University of Notre Dame.

[22] Hermle, M., Létay, G., Philipps, S. P., & Bett, A. W. (2008). Numerical simulation of tunnel diodes for multi- junction solar cells. *Progress in Photovoltaics: Research and applications*, *16*(5), 409–418. https://doi.org/10.1002/pip.824

[23] Sze, S. M., & Ng, K. K. (2006). *Physics of Semiconductor Devices*. Wiley.

[24] Ieong, M., Solomon, P. M., Laux, S., Wong, H.-S., & Chidambarrao, D. (1998). Comparison of raised and Schottky source/drain MOSFETs using a novel tunneling contact model. International Electron Devices Meeting 1998. Technical Digest (Cat. No. 98CH36217), https://doi.org/10.1109/IEDM.1998.746461

[25] Gaspar, G., Serra, J. M., Kern, J., & Müller, M. (2023). TCAD simulation of electrical characteristics of silicon tunnel junctions for monolithically integrated silicon/perovskite tandem solar cells. AIP Conference Proceedings, https://doi.org/10.1063/5.0141125

[26] Synopsys, I. (2018). *Sentaurus™ Device User Guide*.

[27] Shockley, W., & Read Jr, W. (1952). Statistics of the recombinations of holes and electrons. *Physical review*, *87*(5), 835. https://doi.org/10.1103/PhysRev.87.835

[28] Schenk, A. (1992). A model for the field and temperature dependence of Shockley-Read-Hall lifetimes in silicon. *Solid-State Electronics*, *35*(11), 1585–1596. https://doi.org/10.1016/0038-1101(92)90184-E

[29] Sentaurus, T. (2018). Version O-2018.06. *Synopsys, Mountain View, CA, USA*.

[30] Takagahara, T. (1996). Electron—phonon interactions in semiconductor nanocrystals. *Journal of Luminescence*, *70*(1-6), 129–143. https://doi.org/10.1016/0022-2313(96)00050-6

[31] Elnaggar, M., Elogail, Y., Fedawy, M., & Shaker, A. (2026). A Comprehensive Review on III-V TFET Design Optimization. *Micro and Nanostructures*, 208601. https://doi.org/10.1016/j.micrna.2026.208601

[32] Kim, K. (2026). Stacked Si/GaN tunnel junction flip-chip light-emitting diodes with improved external quantum efficiency. *Results in Physics*, 108623. https://doi.org/10.1016/j.rinp.2026.108623